Effects of geological complexities on coseismic displacement: hints from 2D numerical modelling

A. Megna[1], S. Barba[1], S. Santini[2] and M. Dragoni[3]

[1] Istituto Nazionale di Geofisica e Vulcanologia, via di Vigna Murata 605, Roma, Italy

[2] Università degli Studi di Urbino, Istituto di Fisica, via S. Chiara 27, Urbino, Italy

[3] Università degli Studi di Bologna, Dip. di Fisica, Settore di Geofisica, Viale B. Pichat 8, Bologna, Italy

Abstract

By means of a 2D finite-element procedure, we test how heterogeneities at the scale of seismogenic fault affect the displacement. We define one or more slip distributions for two typical normal-faulting earthquakes in the Central Apennines, compute the displacement occurred within different structures, including lateral heterogeneities, and compare the different displacement profiles in order to isolate the effect of the crustal structure. To understand at what magnitude the heterogeneities affect significantly the observation, we compare the predicted coseismic displacement with GPS and DInSAR data for the Colfiorito 1997 earthquake. We find that heterogeneities significantly affect the observable horizontal coseismic displacement for the larger magnitudes, whereas for smaller quakes they affect horizontal displacement close to the fault trace only.

Keywords

fault, numerical models, displacements, heterogeneity, Colfiorito

1. Introduction

Surface displacement induced by faults has been studied at different scales, from the fine structure of the fault zone to the crustal heterogeneities, depending on the observation scale and on the specific problem (see, e.g., Gudmundsson and Brenner, 2003; Zhao *et al.*, 2004). Earthquakes provide us with seismological data to study the causative fault at depth and a sudden displacement at the surface – the effect. Due to poor sampling of data, the coseismic displacement has been often computed assuming homogenous or layered models for the crustal structure in both analytic and finite-element methods. When the data are scarce or inaccurate or when the stratification is poorly known, using simpler models improves the robustness of results obtained by vertical measurements. Differently, horizontal displacements are very sensitive to the presence of low-rigidity layers (Savage, 1998; Cattin *et al.*, 1999; Zhao *et al.*, 2004). As a consequence, wrong fault parameters and slip distribution may derive from inversion of measured displacement when the wrong layering is used.

Today, denser GPS networks of improved technology provide a number of observations of the horizontal displacement. The analysis of these GPS data, separately from or jointly with DInSAR, requires more detailed modelling of the crustal structure, of the earthquake fault, and of the slip distribution. For a 2-D dip-slip fault, we study surface displacements due to different slip distributions and assuming different approximations of the crustal structure.

As a study case, we choose the 1997-98 normal-faulting Colfiorito earthquakes (Central Apennines mountain belt, Italy, Fig. 1), where data disagrees from interpretations (Barba and Basili, 2000). The belt also exhibits horizontal and vertical heterogeneities in the stratification at the length scale of seismogenic faults (Mirabella and Pucci, 2002; Chiarabba and Amato, 2003). The availability of detailed seismic profiles, the occurrence of shallow moderate-magnitude earthquakes, a good record of historical and instrumental earthquakes (up to M7.0, CPTI Working Group, 2004), the long term geological, seismological, and geodetic surveying, and the vast literature available in

the area (Amato and Cocco, 2000, and references therein) provide us a good framework to test how the heterogeneous medium affects the observations.

2. Modelling approach

We build four models with different lithologies assuming uniform slip, and then use several normalized slip distributions in the most complex model to represent how slip distribution influences displacement, accounting also for the fault damage zone. We model two faults capable of typical normal-faulting earthquakes, one large (M6.7), and the other moderate (M6).

2.1 Finite element model

We build the two-dimensional finite-element mesh in a vertical section across the fault by reproducing the detailed geological section of Mirabella and Pucci (2002) (Fig. 2a), using the code MSC.Marc (MSC.Software, 2006).

To isolate the effect of the main seismogenic fault, we reproduce the section including only the most important interfaces. We consider as important such objects (interfaces, lithologies …) whose length is at least $1/10^{th}$ of the seismogenic fault down-dip width (W), and are located close to the fault. We will show that the smallest heterogeneities we accounted for – the turbidites layer - do not affect results. Thus we neglect, as details, smaller heterogeneities and smooth the geometry off of the fault (Fig. 2b). From the section we can easily identify four major lithologic units. From top to bottom, they are Miocene Plio-Plestocene turbidites, Meso-Cenozoic carbonate multilayer, Triassic evaporites, and a Phyllitic Permian-Triassic basement.

The modelled section (300 km length, 100 km depth) has been meshed with four-node quadrilaterals (11.452 elements and 11.735 nodes) (Fig. 2c). The fault lies entirely within the computational domain and cuts the mesh with zero friction slipping edges. Out of the fault zone, surface displacement depends on the final slip and not on friction, and depends very little on the gouge thickness. As for the boundary conditions, the upper surface acts as a stress-free boundary,

whereas the left, right, and bottom edges of the model have been assigned zero displacement in the normal direction.

Our procedure uses variable magnitude forces on the nodes along the fault and orthogonal reaction forces so that the total torque is near zero, as described in Megna *et al.* (2005): the modelled displacement compares well (~5%) to the analytical solution close to the fault trace, i.e. where measures exist, which validates our procedure.

In the Model1, we consider a top layer with average carbonates-evaporites elastic parameters (CA-EV in Table 1) and the basement; in the models 2-4 we use the evaporites and not the average layer; in Model2 we include the carbonates at the top of the evaporites; in Model3 we add the turbidites over the evaporites; in Model4 we incorporate the lateral heterogeneities due to the thrusting (Fig. 3).

Based on P- and S-wave velocity from the literature, we adopt a Young modulus in the range of 8-83 GPa (Table 1). Unfortunately, we do not have access to laboratory values; but we verified that in the South Iceland Seismic Zone in-situ measurements close to the fault yield Young moduli in the lower range of ours (5-10 GPa, Gudmundsson and Brenner, 2003), and the range of seismic velocities is similar (Tryggvason *et al.*, 2002). To account also for such low measurements, we also include in Model4 a fault damage zone (400 m thick, Y=5-10 GPa) .

2.2 Fault parameters

We studied the normal fault of Colfiorito, ruptured during the 1997-98 earthquake sequence. The CMT fault-plane solution of 26 September 1997 mainshock indicates almost pure normal faulting along a ~40° plane dipping toward SW (Ekström *et al.*, 1998). The aftershocks depth distribution is confined between 2 and 9 km (Barba and Basili, 2000; Chiarabba and Amato, 2003), therefore affecting the carbonate multilayer and the evaporites but not the basement (Collettini and Barchi, 2002). Considering these constraints, we define a fault with a dip of 40°, which dislocates the carbonates and evaporites, and its bottom is just over the basement top. We define the two different magnitudes (M6 and M6.7) by setting different fault down-dip width (W=7 and 10 km).

To define the slip, we select arbitrarily some slip distributions in the literature and scale them over the assigned W by using standard relationships (Hanks and Kanamori, 1979; Aki and Richards, 2002) with L/W=1.5-2 and μ=23 GPa (this work) for the Central Apennines.

For the M6.7 earthquake, we consider four slip distributions: uniform slip (US), not uniform slip due to fault-parallel couples of uniform forces acting on the footwall and hanging wall (UF), step-like slip (SL), and symmetrical slip distribution with the maximum value in the centre (CE) (Fig. 4a). All the distributions share the same average slip of 1 m. From the top to the bottom of the fault, we set the slip for SL as 0.4 m (0.8 m; 1.6 m) in a 3 km wide segment (3 km; 4 km); for CE as 0.6 m (1.6 m, 0.6 m) in a 3 km segment (4 km; 3 km), all with the fault top Zt=1 km depth.

For the M6 earthquake, we consider results available in the literature for the Colfiorito earthquake. By inverting geodetic data, many authors (see, e.g., Belardinelli *et al.*, 2004; Hernandez *et al.*, 2004; Lungdren and Stramondo, 2004; Santini *et al.*, 2004) found an asymmetric slip distribution, with the maximum located in the lower half of the fault. For most of them, W ranges between 9 and 10 km, Zt~1 km depth, and the slip averages to ~ 0.4 m. Differently, earthquake locations show that very few or no aftershocks have been reliably located at less than 2 km depth, despite the dense coverage of temporary seismic stations in the area, and that the fault width ranges W~7.5 km (Barba and Basili, 2000) to W~10 km (Chiarabba and Amato, 2003). By analysing the near-source strong motion data of the main shock, Zollo *et al.* (1999) found W=7.5 km, and a nearly uniform slip along the fault – except at the tips of the fault, where the slip rapidly decreases. Considering these constraints, we define for M6 three slip distributions (W=7-10 km, Zt=1-2 km, slip distributions US, AV, TR) with average slip 0.4 m, as showed in figure 4b. In particular, we computed the average slip distribution (AV) from Hernandez *et al.* (2004) and Santini *et al.* (2004).

3. Results

3.1 Case of Magnitude 6.7

We characterise our synthetic case for a M6.7 earthquake with a fault whose parameters are W=10 km, Zt=1 km, and the slip distributions US, UF, CE, and SL with average slip ~1 m.

Comparing the results obtained by fixing the slip distribution US, the horizontal displacement shows variations ranging from 18% to 49% (with the top depth between 1 km and 3 km) (Fig. 5, Zt=1 km case only), causing even greater extension or shortening, as the sign changes across the fault trace. Most of the variation takes place in Model3 and Model4, and it depends by the presence of the low-Young moduli layers at shallow depths. The vertical displacement instead shows some difference (~16%) among the different models 1-4, especially at the maximum subsidence. Contrary to models 1-3, the heterogeneous Model4 exhibits maximum uplift in the footwall.

To understand the effect of the slip in the most complex Model4, we compare the displacements obtained by the slip distributions US, UF, CE, and SL; the vertical displacement pattern due to UF and CE moves to the left and produces a deeper subsidence than US (Fig. 6a). On the contrary, SL pattern shifts more, predicts ~20% less subsidence, and shows longer wavelength than US. The horizontal displacement yields similar results: when the maximum of the slip distribution moves towards the bottom of the fault, the peaks in the horizontal displacement move away from the fault trace, and the wavelength increases (6b).

3.2 Case of Magnitude 6 and comparison with geodetic data

The main question is whether the effect of the crustal model onto the surface displacement can be observed with GPS and/or DInSAR data. We base our M6 synthetic case on the Colfiorito 1997 earthquake, as described in section 2.2. For the three slip distributions, we compare the displacement computed in Model1 and heterogeneous Model4. Results show that the presence of heterogeneities causes little increase of (~1 or 2 cm) footwall uplift (Fig. 7a, US case only). For the subsidence instead the results depend on the slip distribution; the subsidence decreases ~1 cm for US, remains unchanged for AV, and increases ~2 cm for TR. Figure 7b shows the different patterns

of the vertical displacement for the three slip distributions in the case of heterogeneous Model4. Imposing the slip AV or TR, the maximum subsidence moves toward the left direction, and its value increases up to ~30% (~6 cm) with respect to US. The uplift due to AV and TR increases on the hanging wall with respect to US, whereas it does not change above the footwall.

As for the horizontal displacement, the heterogeneities present in Model4 make the extension across the fault trace to increase significantly, like in the M6.7 case (Fig. 8a). For the cases of US and AV, the horizontal displacement increases by ~40% in the footwall and ~15% (1 cm) in the hanging wall. For the TR case, we find ~67% on the footwall and ~27% (2 cm) on the hanging wall. Focusing on Model4, we observe that the cases US, AV, and TR induce a large difference in the horizontal displacement mainly in the hanging wall (Fig. 8b) both in amplitude and wavelength.

We compare the computed displacement with the GPS and DInSAR data recorded in the Colfiorito zone after three moderate magnitude earthquakes (Salvi *et al.*, 2000). The satellite line of sight is near to vertical (~23°), thus we approximate DInSAR data as vertical. In order to partly separate the effect of the three events in the GPS data, we consider only the stations close to the center of the largest fault: PENN (footwall) and CROC (hanging-wall). For the DInSAR data, we make a 4 km-wide box selection across the fault and located in the maximum subsidence zone. In several papers, the final models hardly predict the horizontal displacement at the closest GPS stations, as it is showed in Figure 8a for the model proposed by Hernandez *et al*. 2004. In particular, the homogeneous model predicts a horizontal displacement that is ~50% of observed data at PENN station, which makes the authors to hypothesise a very shallow fault. Differently, we propose that such high values in the measured horizontal displacement may depend on the crustal model. In fact, we show that the presence of the heterogeneities due to thrusting and the use of realistic elastic parameters affect the horizontal displacement by a quantity (up to 100%) that can compensate the misfit obtained in less realistic models (Figs 8a and 8b). We verify that lower Young moduli (5-10 GPa) in the fault damage zone produce ~25% less horizontal displacement at the surface (Fig. 8b): more slip is required to fit the GPS measurements and, as a consequence, the effect of the more

rigid layer increases. Our results suggest that the horizontal displacement strongly depends on the heterogeneities present at depth and that GPS data are likely to show this effect. Differently, large measurement errors (~2.8 cm, Stramondo *et al*., 1999), mostly due to topography (<0.7 cm) and atmospheric effects (1.4 cm, Crippa *et al.*, 2006), prevent us from discriminating among models by using DInSAR (Figs. 7a and 7b).

4. Conclusions

For a typical dip-slip fault in the Central Apennines, we study how the lithological complexities of the crust structure affect surface displacement comparing results obtained in different layered models. We show that the horizontal displacement for the tested fault geometry strongly depends on the elastic stratification, whereas the vertical component does not. This behaviour is also discussed by Savage (1998), Cattin *et al.* (1999), and Zhao *et al.* (2004). By applying different slip distributions, the displacement pattern changes in amplitude and wavelength. When lateral heterogeneities are included, the surface-displacement increases and assumes a shorter wavelength with respect to the layered models, especially in proximity of the fault trace. The position of the maximum subsidence moves towards the hanging wall when different and deeper slip distributions are considered. The wavelength increases when the slip concentrates at depth. The presence of the fault damage zone reduces the expected displacement at the surface, and requires a higher slip to fit the GPS measurements close to the fault trace. Despite the results have been obtained in a 2D model, we carried out our analysis with the data measured close to the fault trace, where 2D and 3D models do not differ significantly. The same conclusions hold for a reverse fault, and can be drawn by reversing the sign of the displacement.

We conclude that for a hypothetical shallow M6.7 earthquake, the heterogeneities significantly affect the surface displacement and have to be accounted for also in the inversion of geodetic data. On the contrary, for a M6 earthquake, the effects on the vertical displacement may be neglected, whereas on the horizontal displacement they may be very subtle and strongly dependent

on the fault depth. We show that the heterogeneities have to be carefully considered in the case of GPS stations close to the fault trace and shallow faults. By neglecting the heterogeneities in such a case, the resulting slip distribution is distorted and the fault appears to be shallower.

References

Aki, K. and Richards, P. G., 2002. Quantitative seismology, 2nd ed., University Science Books. ISBN 978-0935702965.

Alessandrini, B., Filippi, L., and Borgia, A., 2001. Upper-crust tomographic structure of the Central Apennines, Italy, from local earthquakes. *Tectonophysics*, **339**, 479-494.

Amato, A. and Cocco, M. (eds.), 2000. Special issue: The Umbria-Marche, Central Italy, Seismic Sequence of 1997–1998, *J. Seismol.*, **4**(**4**), 5–598.

Barba, S. and Basili, R., 2000. Analysis of seismological and geological observations for moderate-size earthquakes: the Colfiorito Fault System (Central Apennines, Italy). *Geophys. J. Int*., **141**, 241-252.

Barchi, M.R., Minelli, G., and Pialli, G., 1998. The structural style of the Umbria-Marche fold and thrust belt. *Mem. Soc. Geol. It*., **52**, 557-578.

Belardinelli, M.E., Sandri, L., and Baldi, P., 2003. The major event of the 1997 Umbria-Marche (Italy) sequence: what could we learn from DInSAR and GPS data?. *Geophys. J. Int.*, **153**, 242-252.

Cattin, R., Briole, P., Lyon-Cahen, H., Bernard, P., and Pinettes, P., 1999. Effects of superficial layers on coseismic displacements for a dip-slip fault and geophysical implications. *Geophys. J. Int.*, **137**, 149-158.

Chiarabba, C. and Amato, A., 2003. V_p and V_p/V_s images in the M_w 6.0 Colfiorito fault region (central Italy): A contribution to the understanding of seismotectonic and seismogenic processes. *J. Geophys. Res.*, 108, 2248-2264, doi:10.1029/2001JB001665.

Collettini, C. and Barchi, M. R., 2002. A low-angle normal fault in the Umbria region (Central Italy): a mechanical model for the related microseismicity. *Tectonophysics*, **359**, 97–115.

CPTI Working group, 2004. Catalogo Parametrico dei Terremoti Italiani, versione 2004 (CPTI04), INGV, Bologna. http://emidius.mi.ingv.it/CPTI04/

Crippa, B., Crosetto, M., Biescas, E., Troise, C., Pingue, F., and De Natale, G., 2006. An advanced slip model for the Umbria-Marche earthquake sequence: coseismic displacements observed by SAR interferometry and model inversion. *Geophys. J. Int.*, **164**, 36–45 doi: 10.1111/j.1365-246X.2005.02830.x

Di Giulio, G., Rovelli, A., Cara, F., Azzara, R.M., Marra, F., Basili, R., and Caserta A., 2003. Long-duration asynchronous round motions in the Colfiorito plain, central Italy, observed on a two-dimensional dense array. *J. Geophys. Res.*, **108**, 2486, doi:10.1029/2002JB002367.

Ekström, G., Morelli, A., Dziewonski A., and Boschi, E., 1998. Moment tensor analysis of the Umbria-Marche earthquake sequence of September-October 1997. *Geophys. Res. Lett.*, **25**, 1971-1974.

Gudmundsson, A. and Brenner, S., 2003. Loading of a seismic zone to failure deforms nearby volcanoes: a new earthquake precursor. *Terra Nova*, **15**, 187-193, doi: 10.1046/j.1363-3121.2003.00481.x.

Hanks, T.C. and Kanamori, H., 1979. *A moment magnitude scale*. 84 (B5): 2348-50.

Hernandez, B., Cocco, M., Cotton, F., Stramondo, S., Scotti O., Courboulex, F., and Campillo, M., 2004. Umbria-Marche (Central Italy) main shocks from the inversion of GPS, DInSAR and near field strong motion data. *Ann. of Geophys.*, **74**, 1355-1376.

Lundgren, P. and Stramondo, S., 2002. Slip distribution of the 1997 Umbria-Marche earthquake sequence: Joint inversion of GPS and synthetic aperture radar interferometry data. *J. Geophys. Res.*, **107**, 2316, doi:10.1029/2000JB000103.

Megna, A., Barba, S., and Santini, S., 2005. Normal-Fault stress and displacement through finite-element analysis. *Annals of Geophys.*, **48**, 1009-1016.

Mirabella, F. and Pucci, S., 2002. Integration of geological and geophysical data along a section crossing the region of the 1997-98 Umbria- Marche earthquakes (Italy). *Boll. Soc. Geol. It.*, **1**, 891-900.

Morgante, A., Barchi, M-R., D'Offizi, S., Minelli, G., and Pialli, G., 1998. The contribution of seismic modeling to the interpretation of the CROP-03 line. *Mem. Soc. Geol. It.*, **52**, 441-455.

MSC.Software Corporation Home Page, 2006. MSC.Software Corporation - 40 Years of Virtual Product Development Expertise. 21 Jul. 2006 <http://www.mscsoftware.com/>.

Pauselli, C. and Federico, C., 2003. Elastic modelling of the Alto Tiberina normal fault (central Italy): geometry and lithological stratification influences on the local stress field. *Tectonophysics*, **374**, 99-113.

Salvi, S., Stramondo, S., Cocco, M., Tesauro, M., Hunstad, I., Anzidei, M., Briole, P., Baldi, P., Sansosti, E., Fornaro, G., Lanari, R., Doumaz, F., Pesci, A., and Galvani A., 2000. Modeling coseismic displacements resulting from SAR interferometry and GPS measurements during the 1997 Umbria-Marche seismic sequence. *Journ. of Seism.*, **4**, 479-499.

Santini, S., Baldi, P., Dragoni, M., Piombo, A., Salvi, S., Spada, G., and Stramondo, S., 2004. Monte Carlo inversion of DInSAR data for dislocation modeling: application to the 1997 Umbria-Marche seismic sequence (central Italy). *Pure App. Geophys.*, **161**, 817-838, doi:10.1007/s00024-003-2474-1.

Savage, J.C., 1998. Displacement field for an edge dislocation in a layered half-space. *J. Geophys. Res.*, **103**, 2439-2446.

Stramondo, S., Tesauro, M., Briole, P., Sansosti, E., Salvi, S., Lanari, R., Anzidei, M., Baldi, P., Fornaro, G., Avallone, A., Buongiorno, M.F., Franceschetti, G. and Boschi, E., 1999. The september 26, 1997 Colfiorito, italy, earthquakes: modeled coseismic surface displacement from SAR interferometry and GPS. *Geophys. Res. Lett.*, **26**, 883-886

Tryggvason, A., S. Th. Rögnvaldsson, and Ó. G. Flóvenz, 2002. Three-dimensional imaging of the P- and S-wave velocity structure and earthquake locations beneath Southwest Iceland. *Geophys. J. Int.*, **151**, 848–866.

Zhao, S., Müller, R.D., Takahashi, Y., and Kaneda, Y., 2004. 3-D finite-element modelling of deformation and stress associated with faulting: effect of inhomogeneous crustal structures. *Geophys. J. Int.*, **157**, 629-644, doi: 10.1111/j.1365-246X.2004.02200.x.

Zollo, A., Marcucci, S., and Milana, G., 1999. The 1997 Umbria-Marche (central Italy earthquake sequenze: Insights on the mainshock ruptures from near source strong motion records. *Geophys. Res. Lett.*, **26**, 3165-3168.

Acknowledgements

We thank the scientific editor, Prof. Jason Phipps Morgan, and two anonymous referees for their careful review; their suggestions improved the manuscript in both clarity and substance. SB has been partly founded by INGV and Civil Protection Dept.

Figure captions

Figure 1. Central Apennines (Italy). Surface projection of individual seismogenic faults (rectangles; DISS, 2005), thrusts, earthquakes with M>=5.5 (squares; CPTI, 2004), CMTs (http://www.globalcmt.org/, 2006), instrumental earthquakes (grey dots; http://www.ingv.it/~roma/reti/rms/bollettino/), GPS stations CROC and PENN (open triangles), and surface projection of EW geological section (thick line) corresponding to segment AA' in Mirabella and Pucci (2002). In the inset, the rectangle indicates the study area.

Figure 2. (a) Geological section across Colfiorito normal fault, Central Italy (from Mirabella and Pucci, 2002); (b) geometry of the model; (c) enlargement of the mesh. In (b) and (c) the line represents the modelled fault (dashed: W=10 km, Zt=1 km; solid: W=7 km, Zt= 2 km).

Figure 3. The different models (1-4) considered in the text. Elastic parameters are shown in table 1.

Figure 4. Slip distributions. (a) W=10 km, Zt=1 km, solid line: SL, dashed line: US, short-dashed line: CE, dotted line: UF computed in Model4; (b) solid line: AV (Hernandez *et al.,* 2004; Santini *et al*, 2004), W=10 km, Zt=1 km; dashed line: TR (Barba and Basili, 2000; Zollo *et al.*, 1999), W=7 km, Zt=2 km; dotted line: US.

Figure 5. Horizontal displacement in case of US and M6.7 for models 1-4, Zt=1 km, and W=10 km. For all the following figures, the displacement is represented at the free surface, and distances are relative to the fault trace with positive values eastwards (according to figure 1).

Figure 6. (a) Vertical and (b) horizontal displacement for US, UF, SL, CE, W=10 Km in Model4 (Zt=1 km).

Figure 7. Vertical displacement computed for the M6 case. (a) Model1 (dashed line) and Model4 (solid line), slip distribution US, Zt=1 km, W=10 km. (b) Model4 and slip distributions US (solid line), AV (dashed), TR (dotted). DInSAR data (Stramondo *et al*., 1999; Salvi *et al.*, 2000) (crosses; solid: reliable data, empty: unreliable; measurement error ~2.8 cm).

Figure 8. Horizontal displacement computed for the M6 case. (a) Model1 (dashed line) and Model4 (solid line) both with slip distribution AV; displacement computed using Hernandez *et al.* (2004) slip distribution in our Model4 (short-dashed line). (b) Model4 and slip distributions US (solid line), AV (dashed), TR (dotted), TR with Y=10 Gpa (grey dashed line). Crosses: GPS measurements at PENN and CROC sites (Salvi *et al.*, 2000).

Tables

Table 1 - Elastic parameters

layer	Z (km)	V_p (m/s)	V_s (m/s)	ρ (kg/m^3)	Y (Pa) [f]	ν [f]
turbidites	0-1	2300 [a]	1200 [a]	2300 [a]	$8.07 \cdot 10^9$	0.31
carbonates	1-6	5400 [b]	2900 [c]	2600 [e]	$5.67 \cdot 10^{10}$	0.30
evaporites	2-8	6300 [c]	3400 [c]	2800 [e]	$8.38 \cdot 10^{10}$	0.29
basement	>8	5500 [d]	3000 [d]	2840 [e]	$6.59 \cdot 10^{10}$	0.29
CA-EV avg.	0-8	5850	2950	2700	$6.94 \cdot 10^{10}$	0.29

Table 1. Parameters used in the models for the single lithologies or combination of. Vp, Vs: P- and S-wave velocities; ρ: density; Y: Young's modulus; ν: Poisson's ratio; Z: approximate depth range of the lithology; CA-EV: average of carbonates and evaporites. Values taken by a) Di Giulio *et al.*, 2003; b) Morgante *et al.*, 1998; c) Alessandrini *et al.*, 2001; d) Barchi *et al.* 1998; e) Pauselli *et al.*, 2003; f) average elastic parameters Y and ν computed from Vp, Vs, and ρ.

"Figure 1"

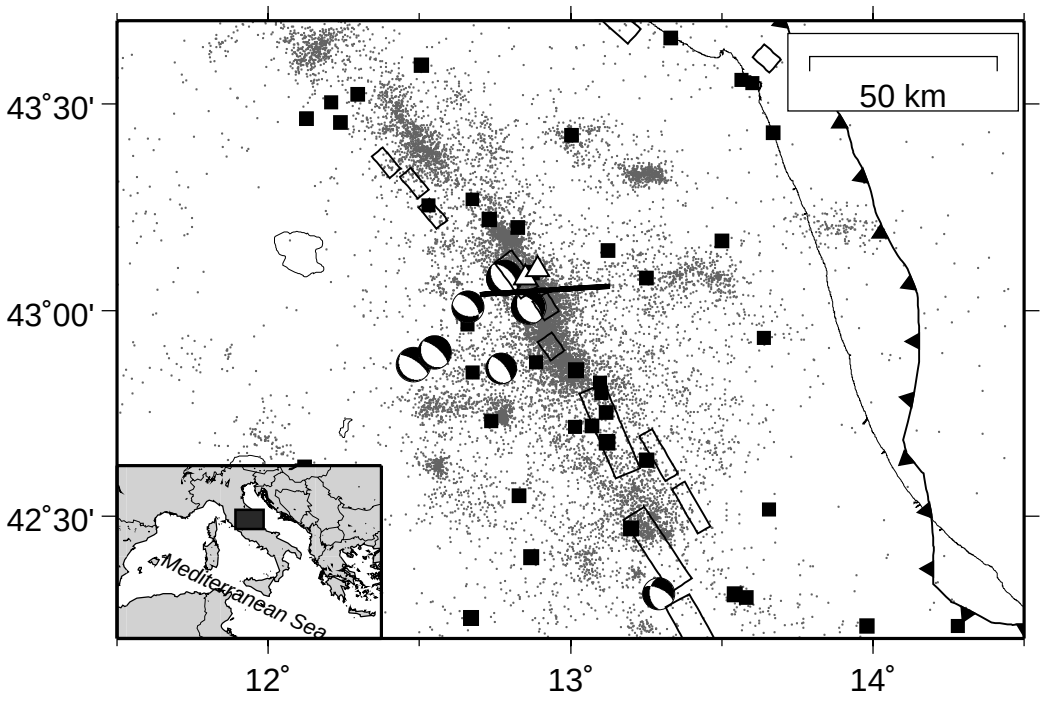

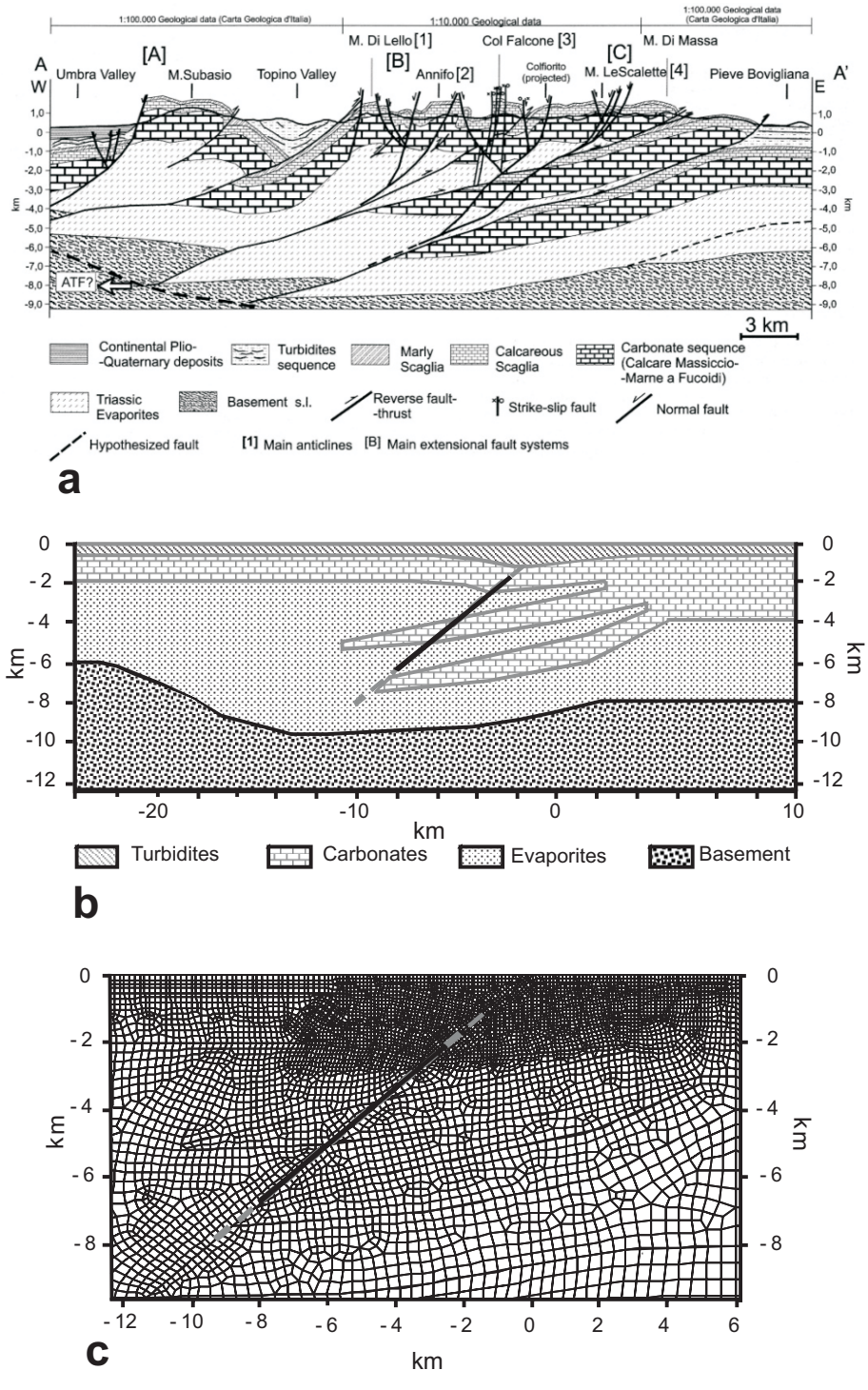
1:100.000 Geological data (Carta Geologica d'Italia)
1:10.000 Geological data
1:100.000 Geological data (Carta Geologica d'Italia)
A
W
[A]
Umbra Valley
M.Subasio
Topino Valley
M. Di Lello [1]
[B]
Annifo [2]
Col Falcone [3]
Colfiorito (projected)
[C]
M. LeScalette [4]
M. Di Massa
Pieve Bovigliana
E
A'
km
ATF?
3 km
Continental Plio- -Quaternary deposits
Turbidites sequence
Marly Scaglia
Calcareous Scaglia
Carbonate sequence (Calcare Massiccio- -Marne a Fucoidi)
Triassic Evaporites
Basement s.l.
Reverse fault- -thrust
Strike-slip fault
Normal fault
Hypothesized fault
[1] Main anticlines
[B] Main extensional fault systems
a
km
-20
-10
0
10
Turbidites
Carbonates
Evaporites
Basement
b
km
-12
-10
-8
-6
-4
-2
0
2
4
6
c

Fig. 2

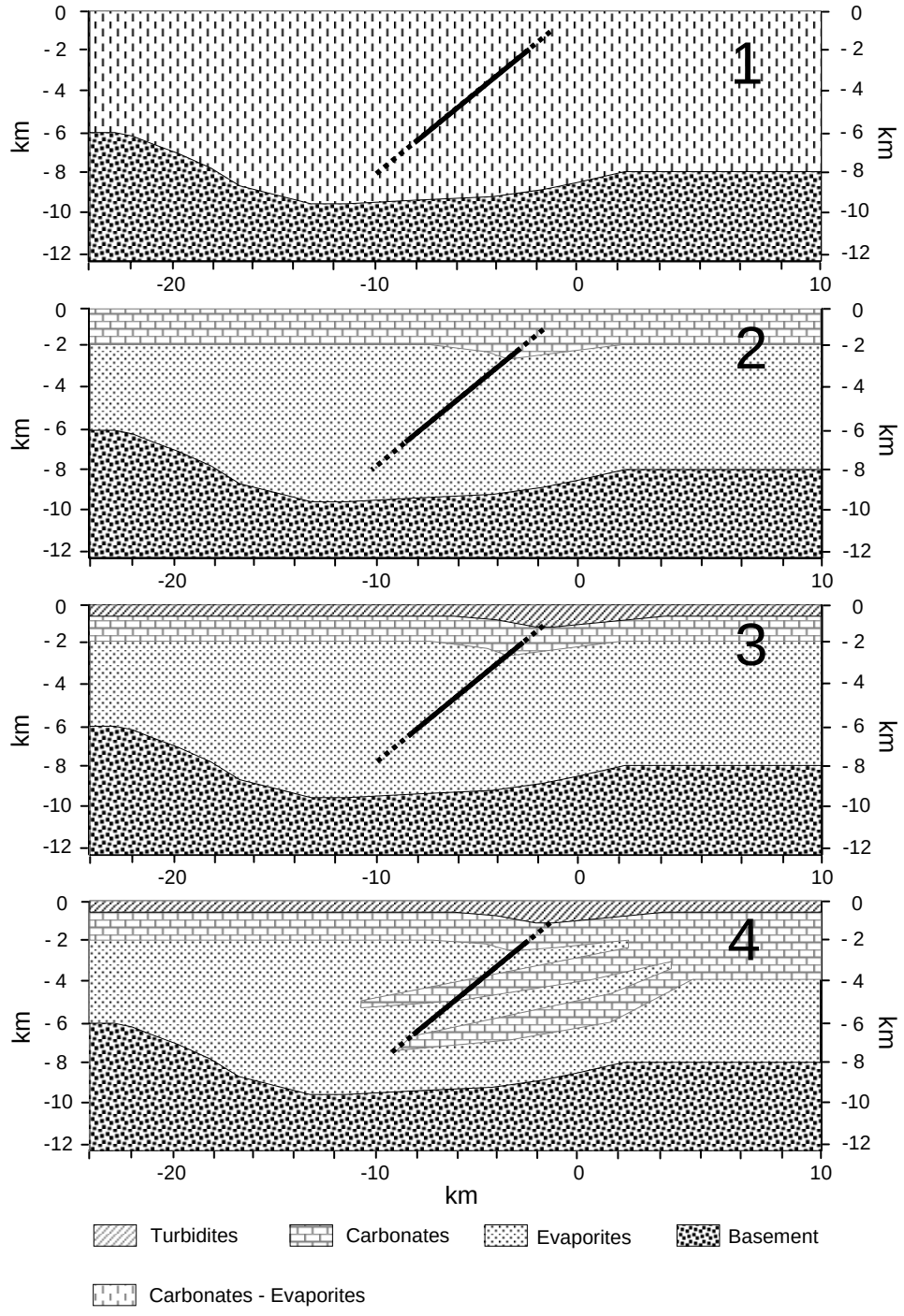
1
2
3
4
km
0
- 2
- 4
- 6
- 8
-10
-12
-20
-10
0
10
Turbidites
Carbonates
Evaporites
Basement
Carbonates - Evaporites

Fig. 3

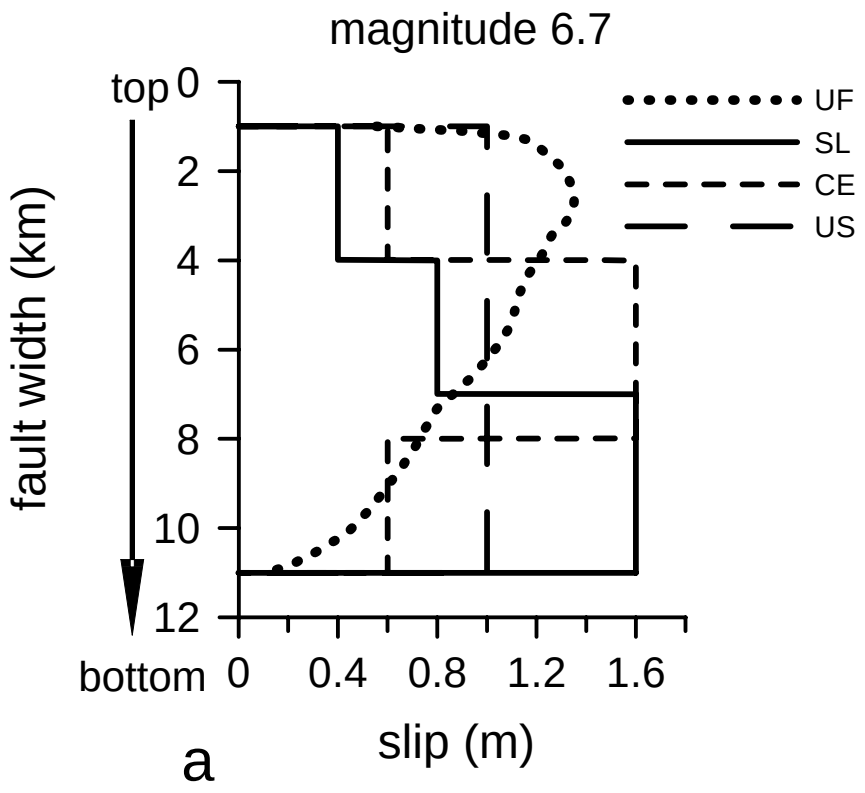
magnitude 6.7
top
bottom
fault width (km)
0
2
4
6
8
10
12
0
0.4
0.8
1.2
1.6
slip (m)
UF
SL
CE
US

a

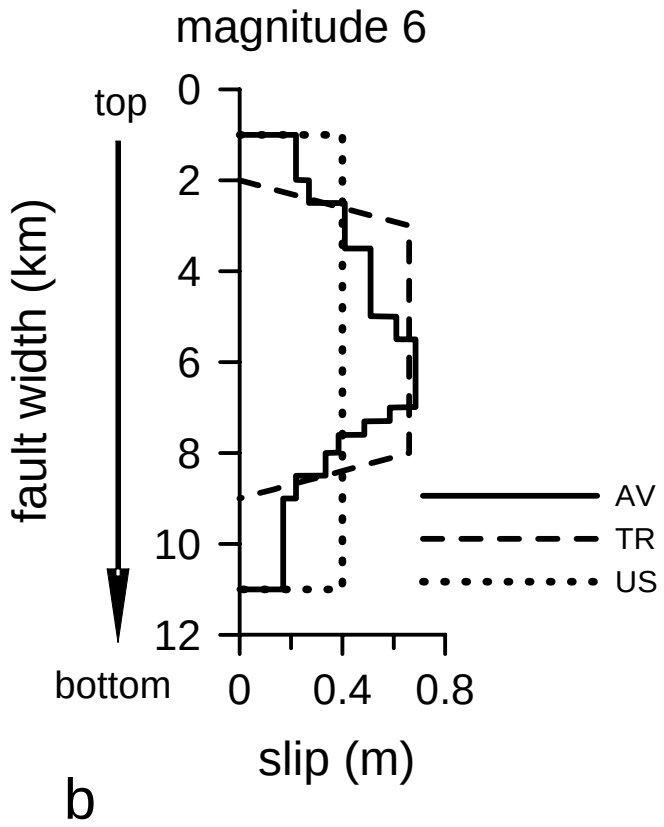
magnitude 6
top
bottom
fault width (km)
0
2
4
6
8
10
12
0
0.4
0.8
slip (m)
AV
TR
US

b

Fig. 4

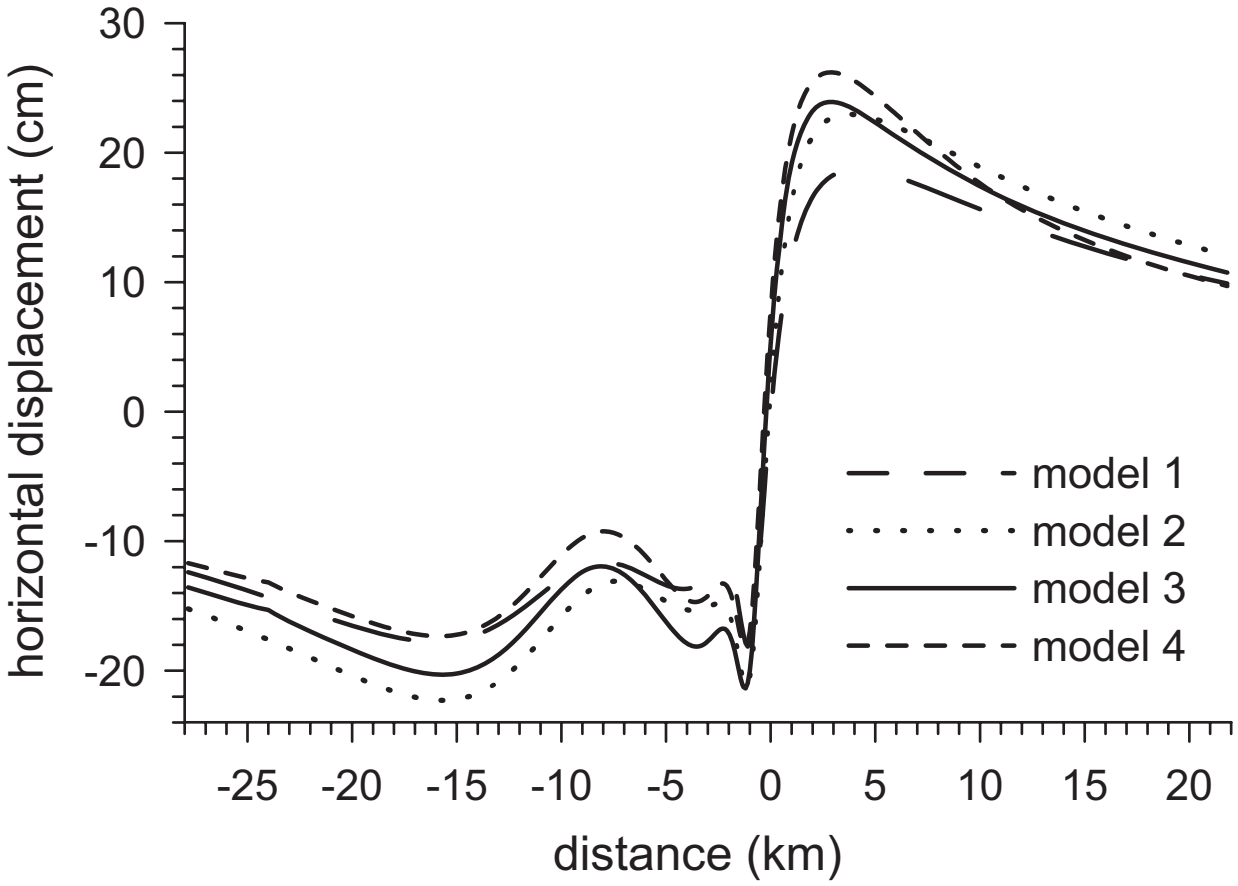
30
20
10
0
-10
-20
horizontal displacement (cm)
-25
-20
-15
-10
-5
0
5
10
15
20
distance (km)
model 1
model 2
model 3
model 4

Fig. 5

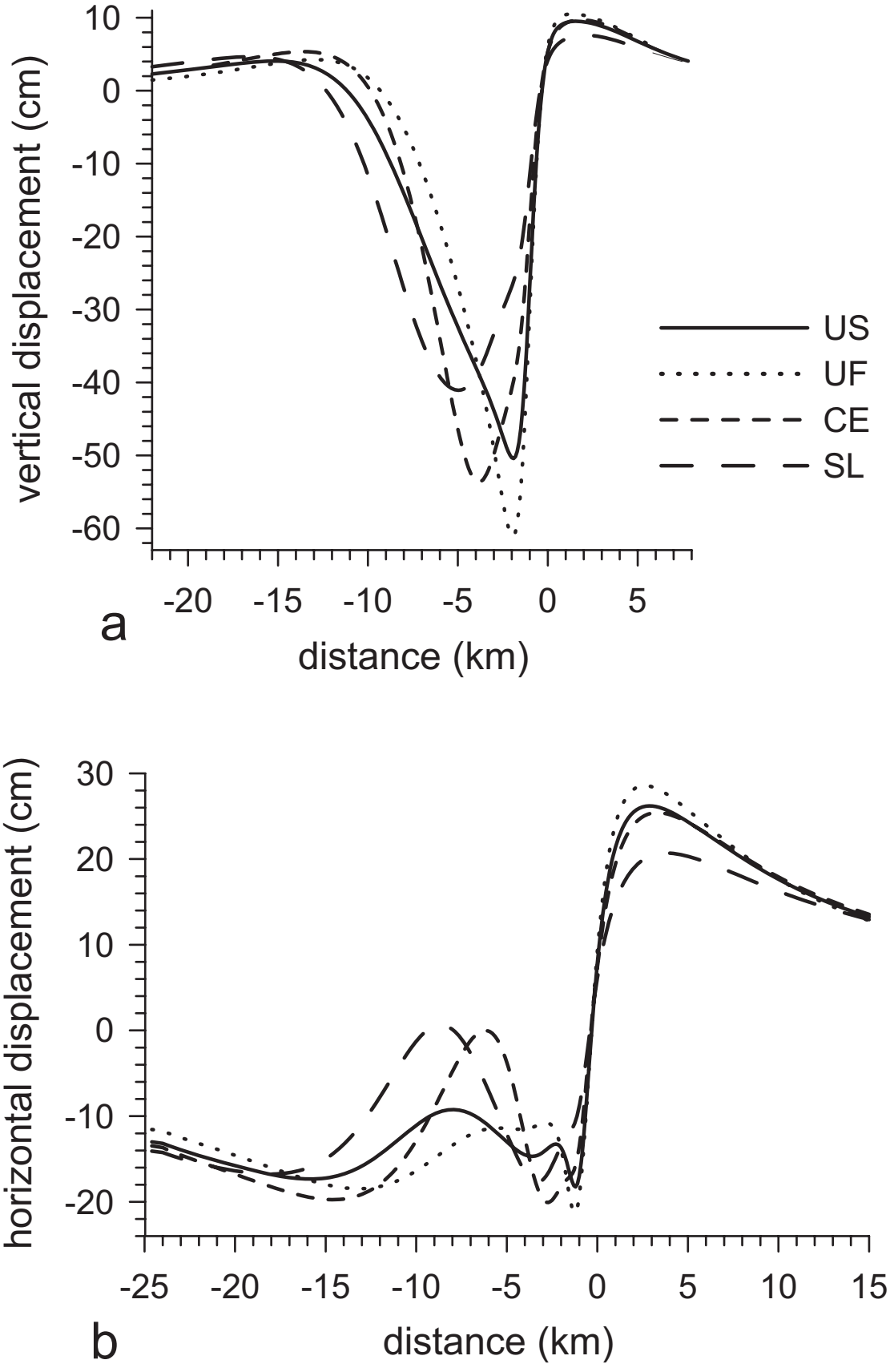
10
0
-10
-20
-30
-40
-50
-60
vertical displacement (cm)
US
UF
CE
SL
-20
-15
-10
-5
0
5
a
distance (km)
30
20
10
0
-10
-20
horizontal displacement (cm)
-25
-20
-15
-10
-5
0
5
10
15
b
distance (km)

Fig. 6

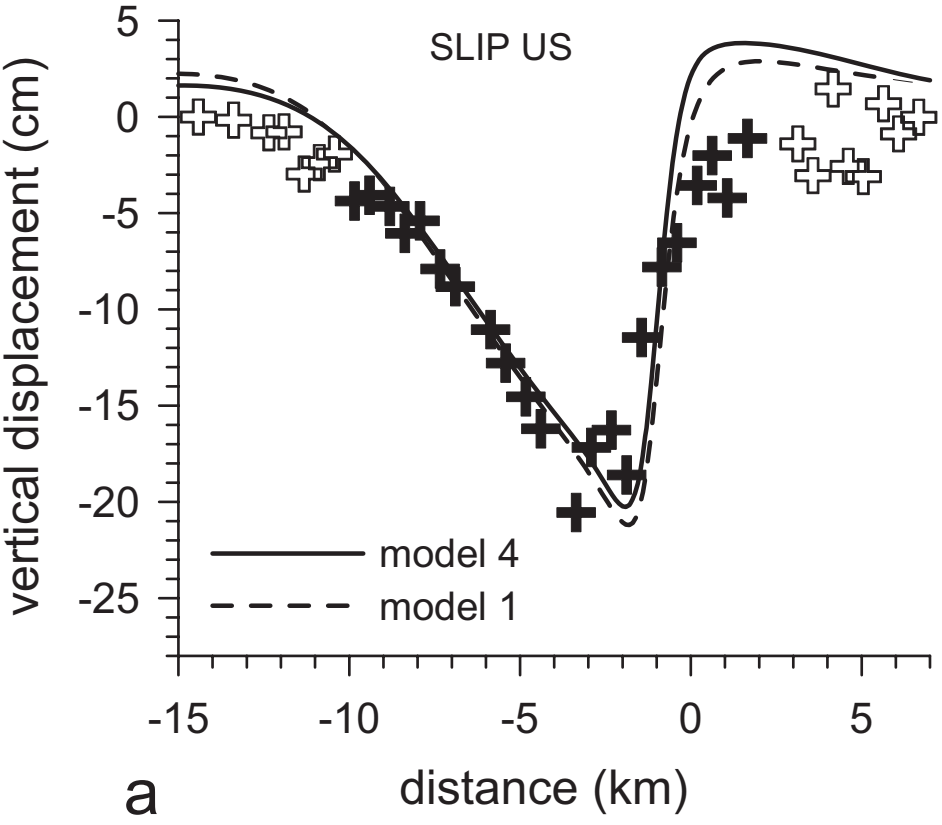
SLIP US
vertical displacement (cm)
5
0
-5
-10
-15
-20
-25
model 4
model 1
-15
-10
-5
0
5
distance (km)
a

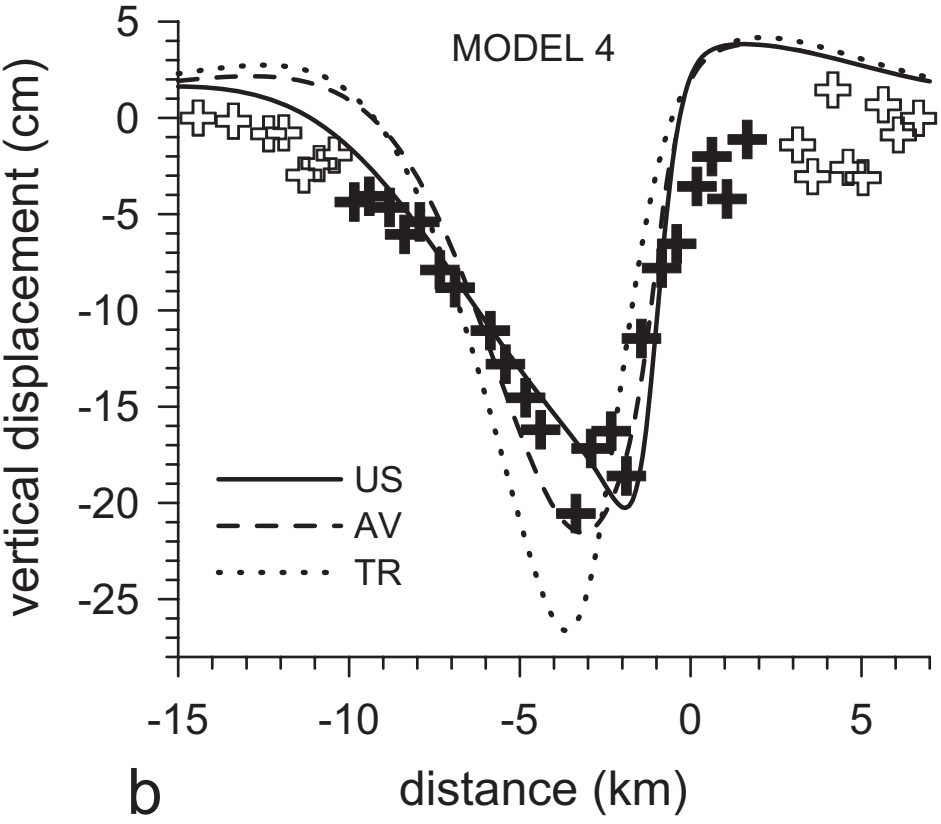
MODEL 4
vertical displacement (cm)
5
0
-5
-10
-15
-20
-25
US
AV
TR
-15
-10
-5
0
5
distance (km)
b

Fig. 7

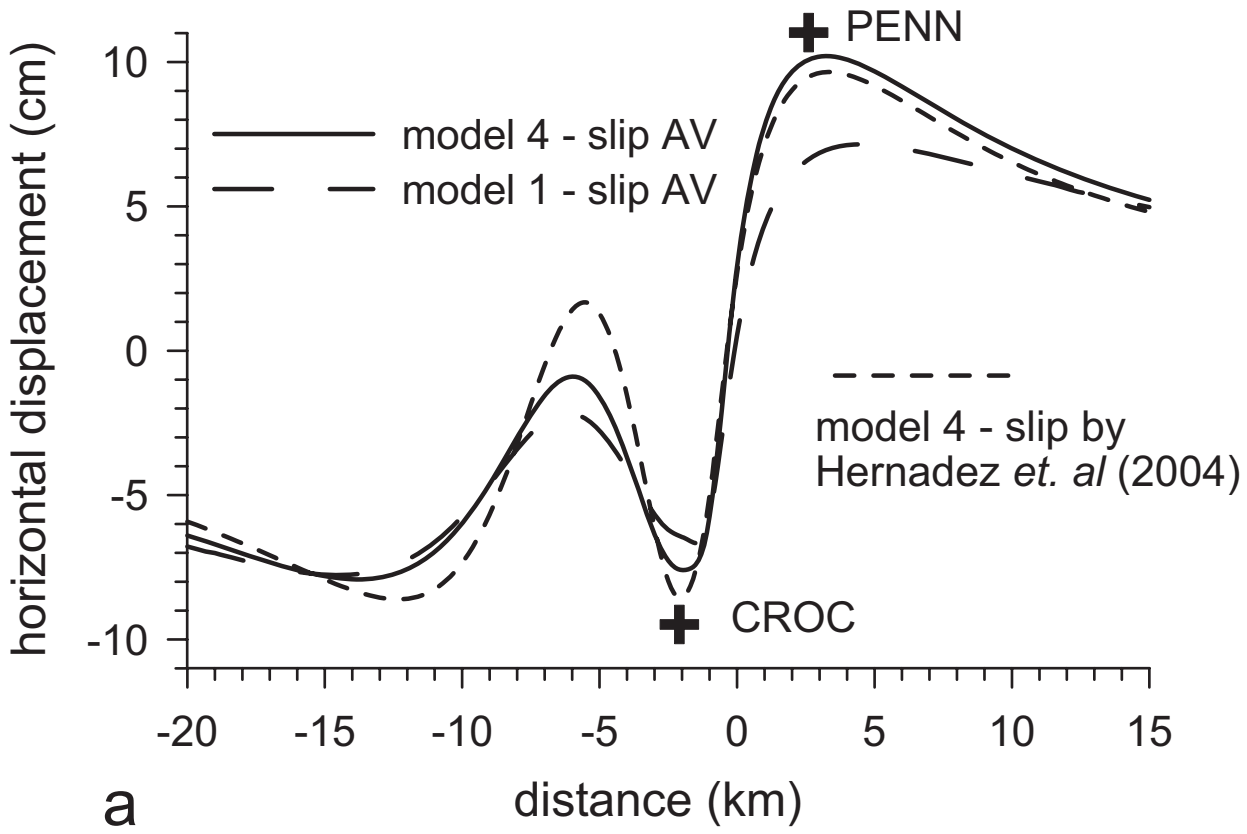
PENN
model 4 - slip AV
model 1 - slip AV
model 4 - slip by
Hernadez et. al (2004)
CROC
horizontal displacement (cm)
distance (km)
a

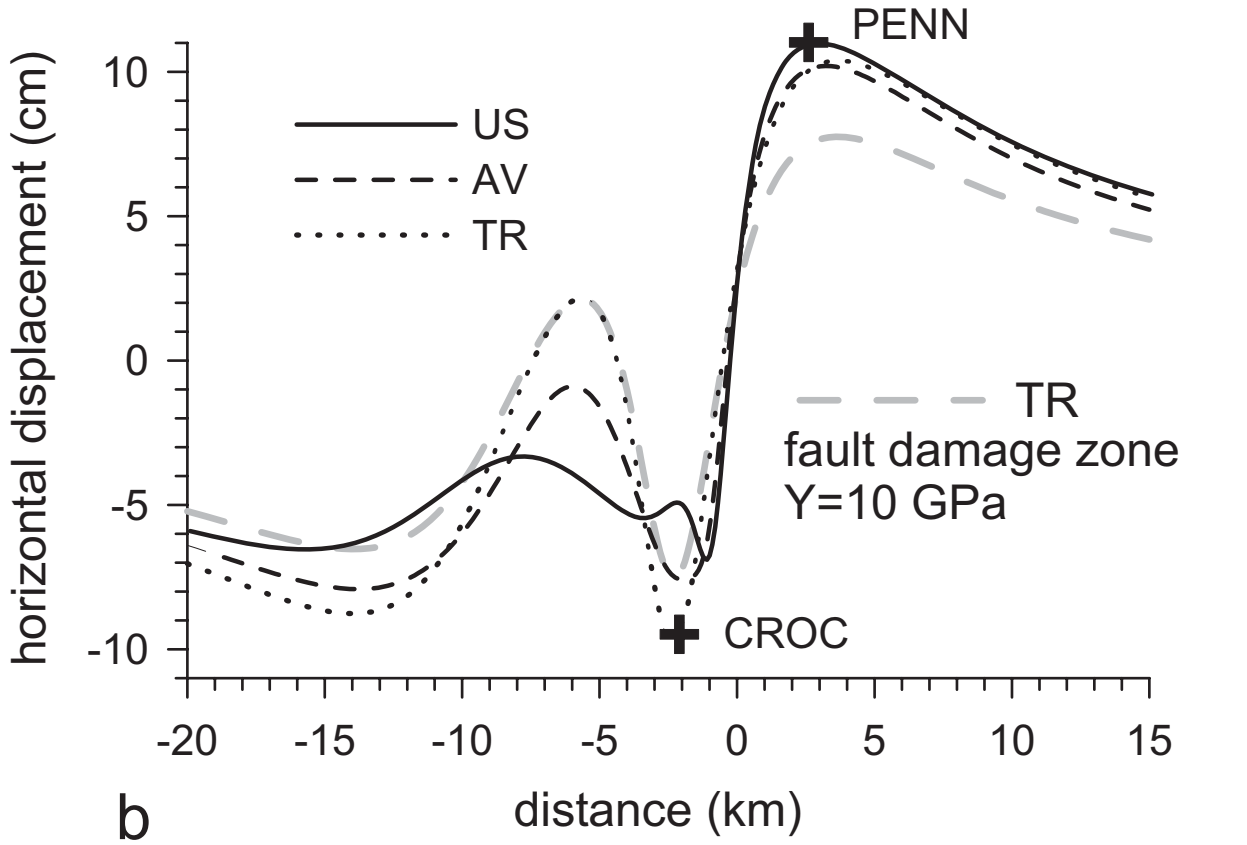
PENN
US
AV
TR
TR
fault damage zone
Y=10 GPa
CROC
horizontal displacement (cm)
distance (km)
b

Fig. 8